ELSEVIER

Polymer 41 (2000) 3719–3727

polymer

The crystallization of poly(aryl-ether-ether-ketone) (PEEK): reorganization processes during gradual reheating of cold-crystallized samples

D.A. Ivanov*, R. Legras, A.M. Jonas

Unité de physique et de chimie des hauts polymères, Université catholique de Louvain, Place Croix du Sud, 1; B-1348 Louvain-la-Neuve, Belgium

Received 7 July 1999; accepted 2 August 1999

Abstract

We have studied by means of X-ray scattering, DMA and densitometry the evolution of the semi-crystalline structure of poly(aryl-ether-ether-ketone) (PEEK) upon reheating specimens initially crystallized isothermally near T_g. Two regimes of reorganization behavior were evidenced. In the low-temperature interval (temperatures below $T_g + \sim 50°C$), the slow dynamics of amorphous segments prevents large-scale rearrangements, strongly limiting the process of reorganization. Only lamellar-scale reorganization occurs, resulting in a slight increase of the crystal thickness and perfection, and in an increase of the constraints in amorphous regions, reflected by an increase of T_g. At higher temperatures, however, a larger-scale melting/recrystallization mechanism sets in. It consists in the recrystallization of whole lamellar stacks to give a state of overall lower free energy, with much thicker and dense crystals separated by larger and less constrained amorphous regions of lower T_g.

Keywords: Relaxation; Crystal reorganization; Semi-crystalline morphology

1. Introduction

The complexity of the thermal behavior of semi-crystalline polymers has been the subject of extensive studies [1–10]. In order to describe the temperature-dependent crystallization or reorganization of the semi-crystalline structure, different models have been proposed [11–16]. Generally, a semi-crystalline structure can be thought of as a metastable system being far from equilibrium [2]. The term "metastable" implies the existence of energetic barriers and related kinetic constraints on the system's path toward equilibrium, i.e. toward a higher degree of crystallinity. Some of the reasons for the metastability of a semi-crystalline structure can be easily grasped. First, it can be related to the topologically complex state of the amorphous interlamellar regions (tight folds, loose loops, tie molecules, etc.) [11], where the entangled amorphous segments are tethered to crystalline surfaces. Second, the metastability can also follow from the out-of-equilibrium (vitreous) state of these disordered inter-crystalline regions, which prevents large-scale reorganization below the corresponding glass transition temperature, T_g. In particular, the latter effect can be of importance for semi-rigid chain polymers, for which the glass transition temperature of inter-crystalline regions is often affected by crystallization [8,17,18], whereas the properties of crystals (e.g., the crystal thermal expansion coefficient) can be influenced by T_g of neighboring amorphous regions [5]. These effects, mainly pertinent to semi-rigid chain polymers, which crystallize only moderately, are related to the interdependence between the properties of amorphous and crystalline regions in the semi-crystalline structure.

In our recent study on the isothermal cold-crystallization of PEEK [19], poly(oxy-1,4-phenyleneoxy-1,4-phenylenecarbonyl-1,4-phenylene), we have observed the progressive disappearance of the α relaxation associated with the glass transition of pure amorphous PEEK (relaxation α_1, glass transition temperature T_{g_1}), and its replacement by another relaxation (α_2, T_{g_2}) located at relatively higher temperatures. During crystallization, the T_{g_2} was gradually increasing; this was attributed to crystal perfection and to formation of new lamellae in some amorphous regions which, despite being already constrained by the presence

* Corresponding author. Laboratoire de Physique des Polymères, CP 223, Université Libre de Bruxelles, Boulevard du Triomphe, 1050 Bruxelles, Belgium. URL: http://www.ulb.ac.be/sciences/polphy/.

E-mail address: divanov@ulb.ac.be (D.A. Ivanov).

0032-3861/00/$ - see front matter
PII: S0032-3861(99)00549-2

of nearby lamellae are of sufficient size to allow the growth of new lamellae (lamellar stack thickening mechanism). Since these mechanisms result in further constraints imposed on the amorphous regions by crystals, an increase of T_{g_2} is concurrent to the increase of crystallinity with time, and its gradual slowing down.

The present work focuses on the details of reorganization of the semi-crystalline structure as a function of annealing temperature and, more specifically, upon progressive reheating of a polymer cold-crystallized near its initial glass transition temperature, T_{g_1}. The objective of this work is to study the interplay between the gradually increasing mobility of the amorphous chains and the driving force of recrystallization, which favors the appearance of thicker crystals as the annealing temperature is increased. For such a study, PEEK is ideally suited, due to its extremely large temperature interval of crystallization ($T_{g_1} = 143$°C, $T_m^0 = 395$°C), high-temperature stability and the absence of polymorphic transitions.

2. Experimental

Sample preparation. Quenched amorphous PEEK sheets (350–500 μm thick) were prepared from dry commercial powder (I.C.I. grade 150P) as described elsewhere [20]. Isothermal crystallization was performed for 3.0 h at $T_c = 153$°C. The degree of transformation achieved at this point corresponds to the full consumption of the inter-spherulitic bulk amorphous material. Subsequently, the samples were reheated stepwise at 1.0°C/min up to different temperatures (T_{cmax}) and quenched to room temperature. The reversibility of the processes occurring during quenching was discussed in Ref. [5] and need not be commented on here. Due to the fact that morphological and relaxation tests were performed after quenching, only irreversible changes in the polymer structure could be detected.

Densitometry measurements were carried out in a density gradient column (water/NaBr), with an accuracy greater than 2×10^{-4} g cm^{-3}. The volume crystallinity was evaluated from a two-phase model, based on estimations[1] for the specific weights of the crystal ($\rho_c = 1.394$ g cm^{-3}) and of pure amorphous PEEK ($\rho_a = 1.264$ g cm^{-3}).

Dynamic mechanical analysis was carried out as described elsewhere [19]. The glass transition temperature (T_g) was determined from isochronal scans (1.0 Hz) as the maximum location of the dynamic mechanical loss modulus.

Small-angle X-ray scattering (SAXS) experiments were performed in an evacuated Kratky compact camera mounted on a Siemens rotating anode generator (Ni-filtered Cu Kα radiation, 40 kV/300 mA). A position-sensitive proportional counter (PSPC, Braun) was used to record the diffraction patterns. The data were first corrected for absorption, parasitic scattering and detector dead time. In a second stage, the data were fitted to the sum of Porod's law and the Ruland's function representing the fluid-like background scattering [21] in the large s-range (0.05–0.1 Å^{-1}):

$$\tilde{i}(s) = \tilde{i}_{Porod}(s) + A_F \exp(Bs^2) \tag{1}$$

with $s = 2\sin(\theta)/\lambda$ where θ is half the angle between incident and scattered beams and λ the X-ray wavelength. In Eq. (1), $\tilde{i}(s)$ stands for the measured (smeared) intensity, A_F and B are constants, and $\tilde{i}_{Porod}(s)$ is a generalized smeared Porod's law taking into account the presence of sigmoidal-gradient density transition layers at crystal boundaries. For our experimental setup, the X-ray beam profile measured in the detector plane was found to be adequately described in its longer dimension by a gaussian of standard deviation $\sigma_{beam} = 0.66$ cm. We thus consistently used the expression of $\tilde{i}_{Porod}(s)$ given by Koberstein et al. [22]:

$$\tilde{i}_{Porod}(s) = \frac{K'}{s^3} \exp(p^2s^2)[(1 - 8\pi^2\alpha^2s^2)\,\mathrm{erfc}(2\pi\alpha s) + 4\sqrt{\pi}\alpha s \exp(-4\pi^2\alpha^2s^2)] \tag{2}$$

where

$$\alpha = [\sigma^2 + (p/2\pi)^2]^{1/2} \tag{3}$$

and

$$K' = \left(\frac{\pi}{2}\right) W_1(0) K_p \tag{4}$$

In Eqs. (2)–(4) σ represents the root-mean-square (RMS) thickness of the density transition layers and K_p is Porod's constant. The parameter p is related to the standard deviation of the beam profile, sample-to-detector distance (SDD) and the X-ray wavelength:

$$p = \lambda\,\mathrm{SDD}/(\sqrt{2}\sigma_{beam}) \tag{5}$$

This parameter allows to describe the beam shape in reciprocal space units as:

$$W_1(s) = W_1(0) \exp(-p^2s^2) \tag{6}$$

The fluid-like background scattering was subtracted from $\tilde{i}(s)$, and these curves were then desmeared using a variant of Glatter's algorithm [23], taking into account the actual profile of the incident beam. The one-dimensional correlation function, $\gamma_1(r)$, was obtained by Fourier transformation of the Lorentz-corrected desmeared intensity. Given the isotropy of our samples, and the lamellar character of semi-crystalline PEEK, s^2 was selected as Lorentz factor. The morphological parameters of the lamellar structure of PEEK, the long period (L) and lamellar thickness (L_c), were obtained from $\gamma_1(r)$ using standard approximate

[1] The crystal density of PEEK is depending on crystallization conditions, and can vary between 1.3665 and 1.4109 g cm^{-3} (Hay JN, Langford JI, Lloyd JR. Polymer 1989;30:489). The value selected in this paper is close to the average value proposed in Jonas A, Legras R. In Kausch HH (Ed). Advanced thermoplastics and their composites. Carl Hanser Verlag, 1992, p. 83.

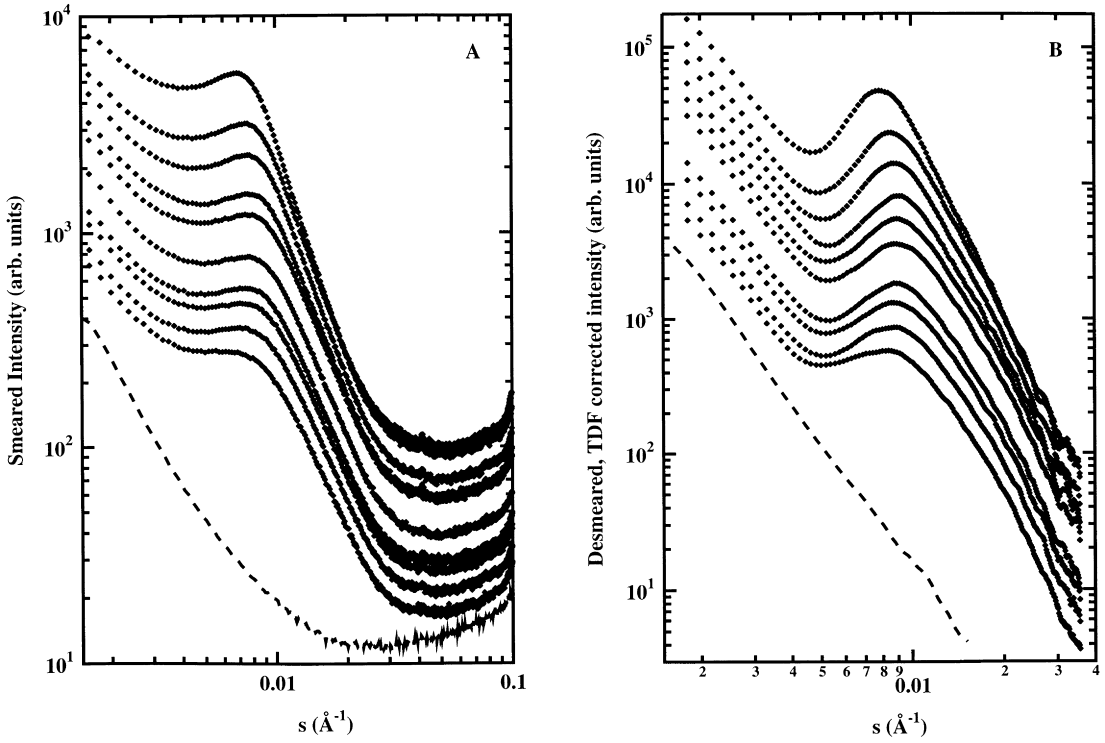

Fig. 1. SAXS data obtained for a PEEK sample isothermally cold-crystallized at low temperature (153°C, 3.0 h) and progressively reheated stepwise to increasingly higher temperature, T_{cmax}. Dotted lines correspond to the initially cold-crystallized sample and to T_{cmax} of 170, 176, 186, 194, 205, 227, 257, 271 and 305°C from bottom to top, respectively. Dashed curves at the bottom of the graphs correspond to the scattering of a fully amorphous PEEK sample. The curves are vertically shifted for clarity. (A) raw data; (B) data after correction for thermal density fluctuations and desmearing.

relationships [24]:

$$\phi_{c,lin}(1 - \phi_{c,lin})L = r_0 \quad (7)$$

$$L_c = \phi_{c,lin}L \quad (8)$$

In Eqs. (7) and (8) $\phi_{c,lin}$ stands for linear crystallinity, L is determined from the location of the first subsidiary maximum of $\gamma_1(r)$, and r_0 is the first intercept of the tangent to the linear part of the correlation function in the self-correlation triangle with the abscissa ($\gamma_1(r) = 0$). In most cases, Eq. (7) provides two values for the linear crystallinity, $\phi_{c,lin}$; we selected the smaller value as the correct one, in agreement with arguments presented elsewhere [5,25–27].

The examination of the width distributions of crystalline and amorphous regions was performed by analysis of the interface distribution functions, $\gamma_1''(r) \equiv d^2\gamma_1(r)/dr^2$, where the derivation is performed over $0 \leq r \leq \infty$. For one-dimensional layered systems, these functions can be related to a series of interfacial distributions [21]:

$$\gamma_1''(r) \propto h_a(r) + h_c(r) - 2h_{ac}(r) + h_{aca}(r) + h_{cac}(r)\ldots \quad (9)$$

In Eq. (9), the subscripts of the distribution functions $h(r)$ indicate what phases (c—crystalline, a—amorphous) should be traversed while calculating the interfacial distance.

Wide-angle X-ray scattering (WAXS) patterns were collected in transmission between 13.5 and 26.4° (2θ) in an evacuated Kratky camera with a reduced sample-to-detector distance. Given the selected geometry, our position-sensitive proportional counter had an effective angular step of 0.033°. The diffractograms were absorption-corrected, then numerically corrected to remove the parallax error of the detector [28] and the effects due to the finite widths of the sample and the detector window. We checked that the corrected data were identical to data acquired with a classical diffractometer working in the Bragg–Brentano reflection geometry. Using our modified Kratky setup for collecting the WAXS allowed to decrease collection times by a factor of 100 as compared to our classical diffractometer, while at the same time allowing to decrease sample size. The desmeared patterns were fitted to a linear superposition of Pearsons distributions of type VII and third order [29] representing the crystalline reflections, plus an empirical function representing the amorphous halo. A crystallinity index ($A_{c,WAXS}$) was obtained by ratioing the area under the crystalline peaks to the total area in the range $2\theta = 13$–27°. For some samples, experiments were also performed in reflection with a Siemens D5000 diffractometer fitted with a graphite secondary monochromator. All the SAXS and WAXS measurements presented here were performed at room temperature.

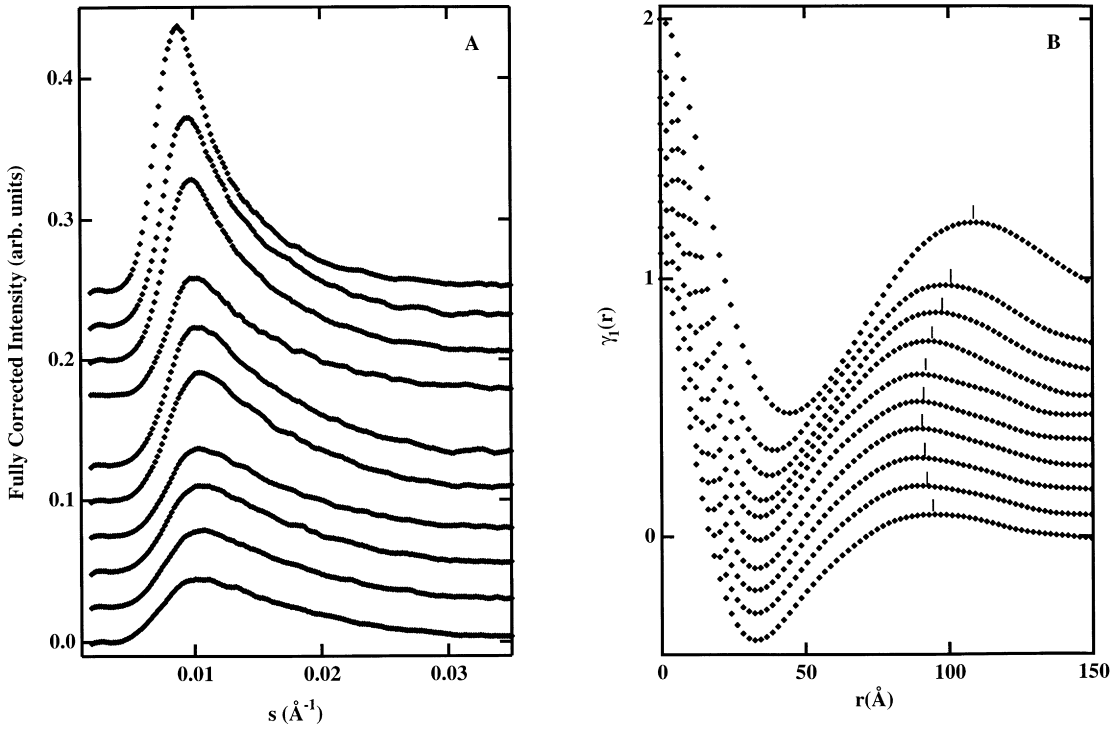

Fig. 2. Continuation of the SAXS data treatment from Fig. 1: (A) fully corrected curves; (B) one-dimensional correlation functions. The designations are as in Fig. 1.

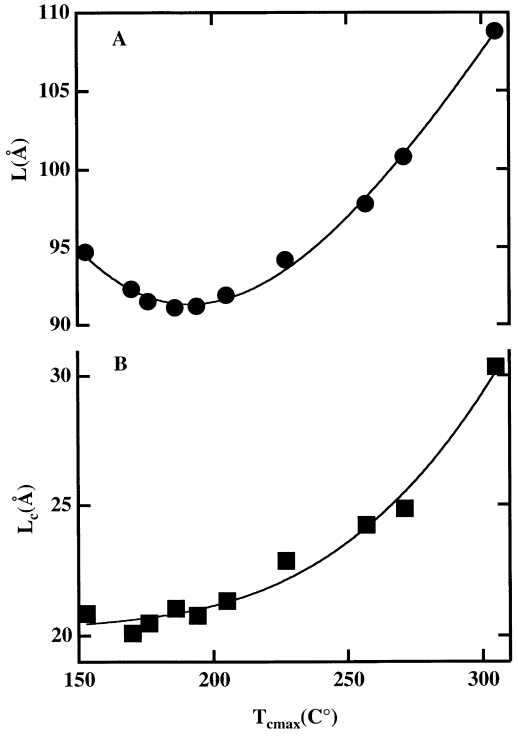

Fig. 3. SAXS morphological parameters as a function of annealing temperature, T_{cmax}, obtained from a simple analysis of one-dimensional correlation functions (Fig. 2b): (A): long period L (●); (B): crystal thickness L_c (■). The lines are guides to the eye.

3. Results

3.1. SAXS measurements

Fig. 1A and B shows the SAXS curves corresponding to a sample of semi-crystalline PEEK gradually reheated to higher temperatures after a long isothermal crystallization in the vicinity of T_{g_1}. The raw data (Fig. 1A), as well as the curves corrected for thermal density fluctuations and subsequently desmeared (Fig. 1B), show a maximum for s-values around 0.008 Å^{-1}. This maximum corresponds to the long periodicity of the electron density inside lamellar stacks. In order to evaluate the structural parameters of the system, the curves were corrected for the central scattering (already present in fully amorphous PEEK), similar to the procedure described in Ref. [27], multiplied by a Lorentz factor s^2 (Fig. 2A) and finally Fourier-transformed (Fig. 2B) using standard extrapolations of the scattered intensity in the low- and high s-ranges. The long period (L) and the crystal thickness (L_c) were then evaluated from the so-obtained one-dimensional correlation functions by means of the approximate equations given in Section 2. The dependence of these parameters on reheating temperature, T_{cmax}, is shown in Fig. 3A and B. Some decrease of L is observed for the values of T_{cmax} below ~200°C, while L_c slightly increases. However, the behavior of both parameters is dramatically changed for higher values of T_{cmax}: above approximately 220°C they start to significantly increase with increasing T_{cmax}. For reasons that will be clarified

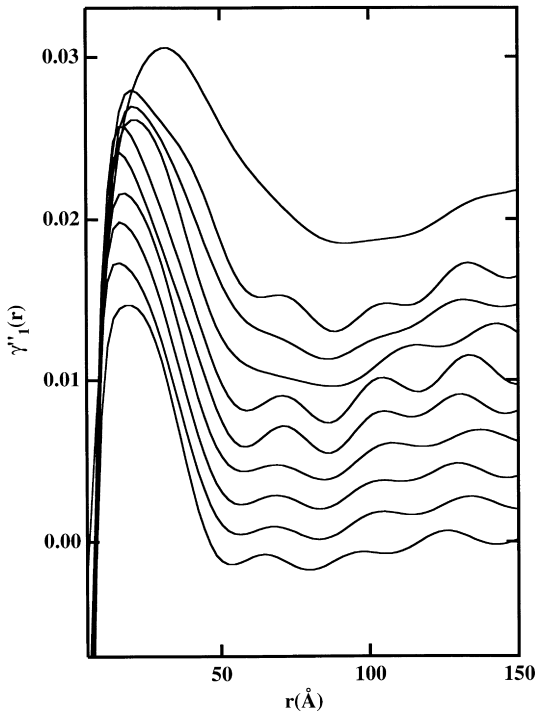

Fig. 4. Experimental interface distribution functions obtained from one-dimensional correlation functions (Fig. 2B). The sequence of the curves is as in Fig. 2.

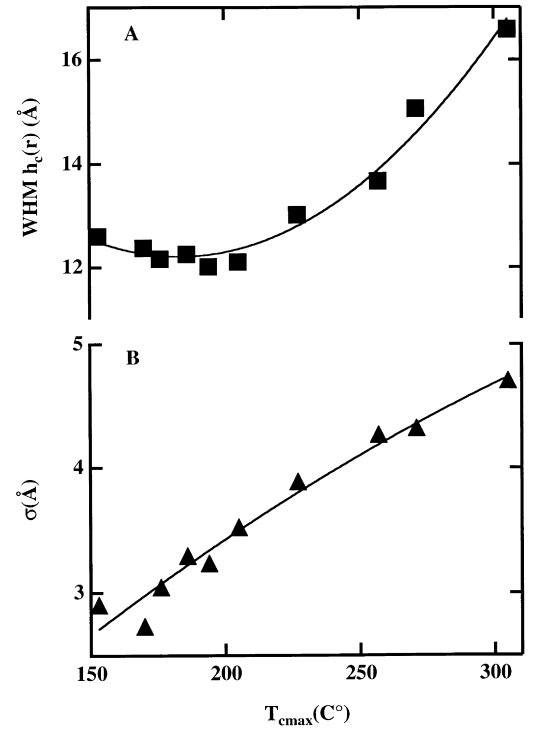

Fig. 5. (A) Width at half maximum of the crystal thickness distribution function, $h_c(r)$, evaluated from the interface distribution functions (Fig. 2b), as a function of T_{cmax}; (B) RMS thickness of sigmoidal-gradient density transition layers obtained from fits of the experimental data (Fig. 11) to a generalized Porod's law as a function of T_{cmax}.

later we denote the first temperature interval ($T_{g_2} < T_{cmax} < T_{g_2} + \sim 50°C$) as "relaxation-controlled" and the second ($T_{cmax} > T_{g_2} + \sim 50°C$) as "recrystallization-controlled" ranges, where $T_{g_2} \sim 160°C$. The relaxation-controlled range roughly corresponds to the increasing branch of linear growth rates versus T_c [30] or, equivalently, to the decreasing branch of peak crystallization times [31] or half-crystallization times versus T_c [32].

Further analysis of the PEEK structural parameters was performed on the basis of the experimental interface distribution functions, $\gamma''_1(r)$, presented in Fig. 4. A strong maximum centered on about 20 Å, is observed for all experimental curves. This maximum can be attributed to the crystal thickness (cf. Figs. 3B and 4); this choice is in line with arguments presented in Refs. [25–27,33]. It should be noted that the distribution functions of the amorphous inter-crystalline distance, $h_a(r)$, and of the long spacing, $h_{ca}(r)$, which should be associated with a maximum and a minimum around 70 and 90–110 Å, respectively, cannot be detected with certainty from the $\gamma''_1(r)$ dependencies (Fig. 4). This is because the average values of L_a and of $L_a + L_c = L$ are too close as compared to the width of the distributions. By contrast, the significant difference between the most probable values for L_c and L_a (at least for annealing temperatures below 305°C) allows to discriminate easily $h_c(r)$. Hence, one can go a step further in the quantitative analysis and estimate the width at half maximum (WHM) of the crystal thickness distribution, WHM $h_c(r)$, (Fig. 5A). One can notice that the behavior of the WHM $h_c(r)$, as a function of T_{cmax}, is very similar to that of L and L_c. In this case, again two temperature regions of different behavior can be detected, with the parameter WHM $h_c(r)$ increasing more rapidly at high annealing temperatures. By contrast, the thickness of the density transition layers, σ, obtained from the fits of the experimental curves to a generalized Porod's law is monotonically increasing throughout the complete temperature range (Fig. 5B), without displaying any specific behavior. It should be noted that σ affects in a negligible way our evaluation of WHM $h_c(r)$, since $\sigma \ll$ WHM $h_c(r)$. Had this been not true, we would have had to consider the convolution of $h_c(r)$ with the function $\exp(-4\pi\sigma^2 s^2)$ in the $\gamma''_1(r)$ function.

3.2. WAXS measurements

Complementary results on the evolution of the semi-crystalline structure of PEEK were obtained from WAXS. It is well documented [5,34–36] that the unit cell dimensions a and b of PEEK are decreasing with increasing T_c. Therefore, we could use them also as indicators for the structural evolution of the system. Fig. 6 presents the values of a, b and the full width at half maximum of the 200 reflection ($FWHM_{200}$, 2θ) versus T_{cmax}. The general trends are very similar to those of L and L_c (Fig. 3): in the relaxation-controlled range a and $FWHM_{200}$ are almost constant; by contrast, they evolve more rapidly above 220°C. It

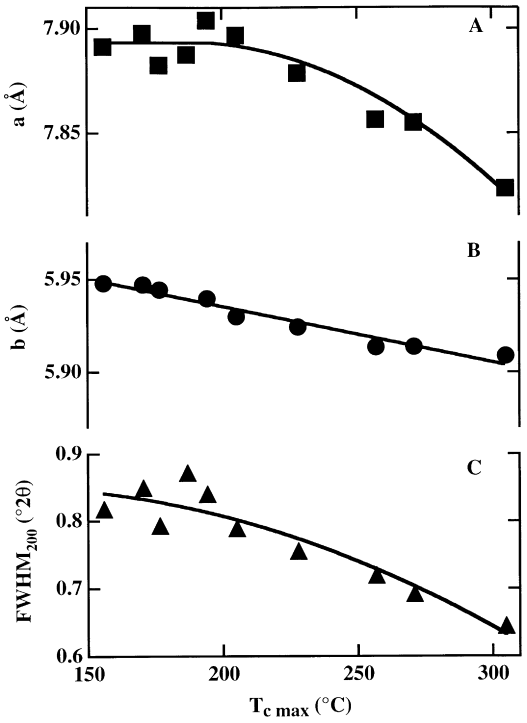

Fig. 6. Evolution of the WAXS structural parameters with T_{cmax} for the PEEK sample described in caption to Fig. 1: (A) a (unit cell parameter); (B) b (unit cell parameter) and (C) full width at half maximum of the 200 reflection ($FWHM_{200}$).

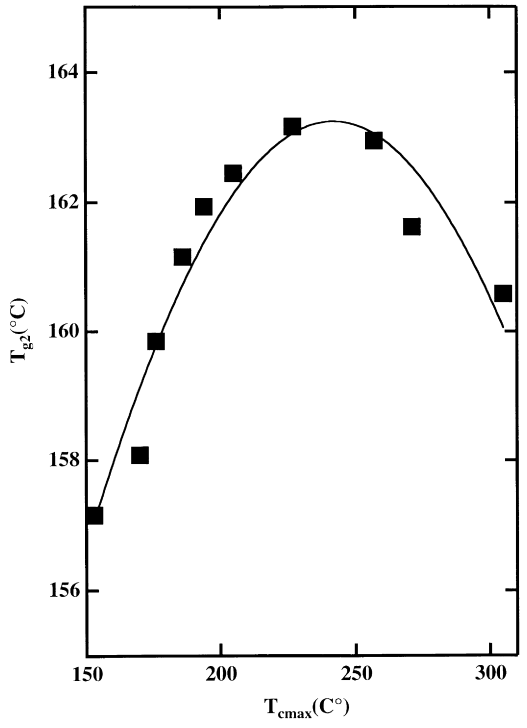

Fig. 7. T_{g_2} versus T_{cmax} for the PEEK sample described in caption to Fig. 1. The lines are guides to the eye.

Table 1
Structural and relaxation parameters of a PEEK sample initially crystallized for 3.0 h at 153°C, then progressively reheated stepwise to increasingly higher T_{cmax}

T_{cmax} (°C)	ρ (g/cm^3)	ϕ_c [a]	$\phi_{c,lin}$ [b]	$A_{c,WAXS}$ [c]	T_{g_2} (°C)
170.6	1.2868	0.191	0.21(8)	0.185	158.1
176.8	1.2884	0.203	0.22(4)	0.191	159.9
186.9	1.2902	0.217	0.23(1)	0.211	161.2
194.3	1.2908	0.221	0.22(8)	0.225	162.0
205.1	1.2929	0.237	0.23(2)	0.222	162.5
227.9	1.2952	0.255	0.24(2)	0.241	163.2
257.6	1.2986	0.282	0.24(7)	0.282	163.0
271.4	1.2992	0.286	0.24(6)	0.286	161.6
305.5	1.3046	0.328	0.27(9)	0.320	160.6

[a] Densitiometric crystallinity.
[b] SAXS linear crystallinity.
[c] WAXS index of crystallinity.

should be noted that $b(T_{cmax})$ does not exhibit this characteristic break in the slope and behaves quite linearly in the complete temperature interval (Fig. 6B). Note in this respect that a is usually more sensitive to the change of crystallization temperature [5,34–36].

3.3. DMA and densitometry measurements

The relaxation properties of the interlamellar amorphous regions were studied by DMA. The dependence of the glass transition temperature of these regions, T_{g_2}, on T_{cmax} is given in Fig. 7. One can see that once again two regimes of thermal behavior can be clearly distinguished. However, in this case, this parameter is increasing in the relaxation-controlled range, while it shows a more limited decrease in the recrystallization-controlled range. The comparative evolution of the densitometric crystallinity, the SAXS linear crystallinity and the WAXS index of crystallinity are summarized in Table 1. The parameters related to crystallinity clearly reveal the same type of temperature evolution as the structural parameters discussed earlier: only a relatively small variation is detected at low annealing temperatures, while a strong increase is observed at higher temperatures.

Concluding, a clear relationship between the evolution of the parameters describing the morphology of the semi-crystalline structure, crystallinity and relaxation is observed while reheating a cold-crystallized PEEK sample; this phenomenon will be discussed in the rest of this work.

4. Discussion

We will open this section with two important remarks. Firstly, our experiments exclude the time variable from consideration. This is because our heating rate corresponds to a unique characteristic time that was not varied in the present work. As a consequence, we can only observe reorganization processes which occur within this characteristic

time; slower processes will be overlooked in this study. This could be especially important at very high and very low T_{cmax} when the growth rates are small. However, in the present work, we will not use T_{cmax}s close to the final melting point. Moreover, for the lower T_{cmax}s, we will be able to use the results gained in our previous isothermal cold-crystallization study [19] that was performed for long crystallization times.

Secondly, we will not consider in this paper the question of the spatial distribution of the reorganization processes that occur. For this purpose, only direct-space investigations performed on the elements of the semi-crystalline structure are adequate. Such microscopy studies were reported elsewhere [37].

4.1. Relaxation-controlled range

In our previous work [19] on the isothermal crystallization of PEEK at 156°C we showed that the dynamics of the later stage of crystallization was controlled exclusively by mechanisms acting inside the spherulites. Moreover, at this stage of crystallization, very little variation of the morphology could be observed with time. This was ascribed to the progressive blocking of reorganization processes (stack thickening and perfection of crystals) due to the decreased mobility of nearby amorphous interlamellar regions (detected by a progressive increase of T_{g_2}). Taking into account the vicinity of the glass transition region, we may thus describe the semi-crystalline structure at the end of the isothermal experiment by a model including crystalline zones more-or-less isolated from each other by small regions of frozen amorphous polymer.

Now, suppose that we start to reheat this system. Then some of the imperfect crystallites formed at large undercoolings could be able to undergo partial melting. However, if we are still in the temperature interval where the characteristic relaxation time of the amorphous segments is significant as compared to the characteristic recrystallization time, no large-scale rearrangements will be able to occur during the heating. Each lamella will behave as if more or less independent of its crystalline neighbors in the lamellar stack. Therefore, all the reorganization processes will remain restricted near to the lamellar scale. This lamellar-scale reorganization is evidenced by a slight increase of L_c (Fig. 3B), a small densification of the crystals (decrease of b, Fig. 6B), a slight increase of crystallinity (densitometry and WAXS data, Table 1) and, accordingly, by a monotonic increase of the thickness of the density transition layers (Fig. 5B). In this range, a very small decrease of L can also be detected, which could be accounted for by variation in the coherence of the lamellar stacking [19]. Hence, in this temperature range, we associate the evolution of the semi-crystalline structure to the reorganization of the sample at the scale of individual lamellar crystals, which exerts further constraints in adjacent amorphous regions, thereby increasing their T_g. The progressive and localized crystal perfection in this temperature range should then be explained by a competition between the recrystallization of crystallites and the blocking of the segments by the sluggish amorphous interlayers. This blocking mechanism is one of the reasons why the reheated semi-crystalline structure preserves an out-of equilibrium state quite similar to its initial state, as is evidenced by the very small evolution of the morphological parameters. Thus, in this temperature range, the morphological memory of the semi-crystalline structure is partially explained by the low mobility of amorphous segments in interlamellar regions.

4.2. Recrystallization-controlled range

If we further heat the sample, the role of the relaxation parameters of the amorphous matrix will become less important. Therefore, we could expect a larger-scale reorganization process to take place, with coordinated rearrangements occurring in neighboring crystals, also reorganizing. This is indeed what can be observed experimentally via the increase in the slopes of dependencies of L, L_c, WHM $h_c(r)$, a, $FWHM_{200}$ versus T_{cmax} (Figs.3A, B, 5A, 6A, C). In this case, it is clear that such a dramatic evolution of the parameters of the semi-crystalline structure cannot happen without the reconstruction of a significant amount of the pre-existing lamellar stacks. In particular, it is impossible to imagine that a simultaneous increase of crystallinity and long period occurs without a substantial reorganization of all the space-filling semi-crystalline structure. As concerns the crystal perfection process, a similar conclusion can be obtained from the examination of the shapes of the interface distribution functions shown in Fig. 4, as a function of the annealing temperature. It can be seen in the crystal thickness distribution that thicker crystals appear as T_{cmax} increases in the recrystallization-controlled range. These thicker crystals promote a progressive broadening of the distribution functions, finally, for the highest annealing temperature, the crystal thickness distribution shifts as a whole toward larger values. Thus, the majority of the lamellar stacks and lamellar crystals evolve during reheating and reorganize in a new state of different morphological parameters and different unit cell dimensions. Accordingly, we interpret the progressive decrease of the breadth of the 200 reflection (Fig. 6C) either as the enlarging of the lateral size of coherently scattering domains due to the recrystallization, or as the increase of the crystal perfection due to the decrease of paracrystalline distortions of the lattice [38].

From the point of view of spatial distribution and abundance of the reorganizing stacks, atomic force microscopy experiments performed on single PEEK spherulites are in a full agreement with the interpretation presented in this work [37]. These conclusions can be of importance for the interpretation of the thermal properties of PEEK and, in particular, for the understanding of the well-documented double-melting behavior of cold-crystallized PEEK. It should be noted in this respect that our observations are

Table 2
Effective temperature contraction coefficients of the unit cell parameters a and b of PEEK reheated after isothermal cold-crystallization (this work) and crystallized directly at different T_cs (literature data)

	$-da/dT_c$ (Å/K) $\times 10^4$	$-db/dT_c$ (Å/K) $\times 10^4$
Ref. [34]	11.2 ± 2.3	3.5 ± 0.8
Ref. [35]	9.7 ± 1.5	7.4 ± 1.1
Ref. [36]	12.3 ± 1.5	3.6 ± 1.4
Ref. [41]	9.87 ± 0.18	3.37 ± 1.2
This work[a]	6.7 ± 0.3[b]	2.7 ± 0.6

[a] Derivation of *a*,*b* over T_{cmax}.
[b] Evaluation for $T_{cmax} > 205$°C (Fig. 6A).

not compatible with the dual lamellar population models which assume the existence of thinner lamellae (organized either in separate stacks or in mixed stacks with thicker lamellae) that would be the only ones undergoing reorganization upon heating.

Generally, the rate of the system evolution in the recrystallization-controlled range (taken for example as the value of the apparent temperature contraction coefficient of *a*, da/dT_{cmax}) becomes comparable with literature data (Table 2) reported for samples crystallized directly at various T_cs. This means that the morphological memory is now less able to keep the information about the structures formed at large undercoolings. This is in agreement with the larger scale reorganization occurring in this temperature range, sometimes denoted as "melting-recrystallization mechanism" [5,10,39,40].

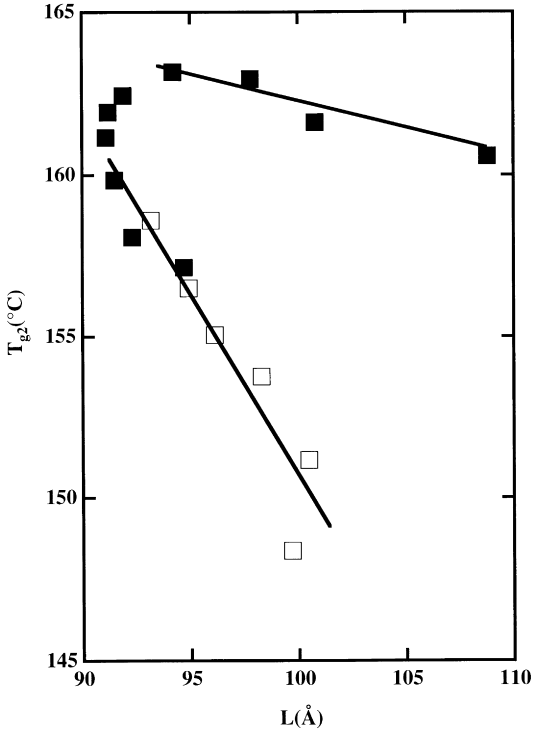

Fig. 8. T_{g_2} versus long period, L, for (1) a PEEK sample crystallized isothermally at $T_c = 156$°C for different times [19] (□), (2) the PEEK sample described in caption to Fig. 1 (■). The lines are guides to the eye.

4.3. Evolution of amorphous versus crystalline regions during reorganization

Our findings concerning the regimes of crystallization/reorganization are supported by a complementary study of the relaxation behavior of the amorphous regions by dynamic mechanical analysis (Fig. 7, Table 1). In the relaxation-controlled range, the glass transition of semi-crystalline PEEK increases strongly with T_{cmax}. By contrast, in the recrystallization-controlled range, a slight decrease of T_{g_2} with T_{cmax} is observed. In order to combine the data characterizing the evolution of the semi-crystalline morphology with the relaxation parameters of the amorphous regions we have plotted the dependence of T_{g_2} versus *L* for both the isothermal crystallization of PEEK [19] and the present study (Fig. 8). The form of this graph confirms the existence of two regimes of crystallization/reorganization. During isothermal cold-crystallization and upon reheating in the relaxation-controlled range the first regime is evidenced by a strong increase of T_{g_2} with almost no variation of *L*. As was stated above for the case of isothermal cold-crystallization, this evolution results from further constraining of the amorphous regions by the local reorganization of almost isolated crystals. However, the second regime is apparent as indicated by a significant increase of *L* with a simultaneous small decrease of T_{g_2}. It corresponds to T_{cmax} being in the recrystallization-controlled range and reflects the partial release of constraints imposed by the crystalline stems in the amorphous regions, due to the reorganization occurring at a larger scale. These constraints become distributed over a larger volume after recrystallization of the lamellar stacks. Therefore we can describe the evolution of the amorphous regions upon reheating as further constraining of the amorphous regions during lamellar scale reorganization, and relaxation of stresses at higher T_{cmax} when recrystallization in a quite different state follows the local melting of the lamellar stacks.

5. Conclusions

The strong coupling between the reorganization of the semi-crystalline microstructure and the relaxation behavior of interlamellar amorphous regions has been clearly shown for PEEK in this work. In the relaxation-controlled range ($T_{g_2} < T_{cmax} < T_{g_2} + \sim 50$°C), the slow dynamics of amorphous segments prevents large-scale rearrangements, strongly limiting the process of reorganization. Only lamellar-scale reorganization occurs, resulting in a slight increase of the crystal thickness and perfection, and in an increase of the constraints in amorphous regions, reflected by an increase of T_{g_2}. At higher temperatures, however, a larger-scale melting/recrystallization mechanism sets in. It consists in the recrystallization of whole lamellar stacks to give a

state of overall lower free energy, with thicker crystals separated by larger and less constrained amorphous regions of lower T_{g_2}.

Acknowledgements

Partial financial support of this work by the Belgian National Fund for Scientific Research (FNRS) is gratefully acknowledged. We also appreciate partial financing of this work in the frame of a "mécénat Sandoz". The authors thank O. Dupont for fruitful discussions about PEEK microstructure, and Dr Do Y. Yoon for his continuing interest in our work.

References

[1] Todoki M, Kawaguchi T. J Polym Sci: Polym Phys Ed 1977;15:1067.
[2] Yagfarov MSh. Polym Sci USSR 1982;24:2915.
[3] Blundell DJ. Polymer 1987;28:2248.
[4] Jonas AM, Russell TP, Yoon DY. Colloid Polym Sci 1994;272:1344.
[5] Jonas AM, Russell TP, Yoon Do Y. Macromolecules 1995;28:8491.
[6] Cebe PJ. Mater Sci 1995;23:3721.
[7] Kruger K-N, Zachmann HG. Macromolecules 1993;26:5202.
[8] Cheng SZD, Cao M-Y, Wunderlich B. Macromolecules 1986;19:1868.
[9] Bassett DC, Olley RH, Raheil IAM. Polymer 1988;29:1745.
[10] Gehrke R, Riekel C, Zachmann HG. Polymer 1989;30:1582.
[11] Mansfield ML. Macromolecules 1987;20:1384.
[12] Sadler MD, Gilmer GH. Phys Rev B 1988;38:5684.
[13] Sadler MD, Gilmer GH. Polymer 1984;25:1447.
[14] Goldbeck-Wood G. J Polym Sci: Part B: Polym Phys 1993;31:61.
[15] Lauritzen JI, Hoffman JD. J Appl Phys 1973;44:4340.
[16] Point JJ. Macromolecules 1979;12:770.
[17] Vigier G, Tatibouet J, Benatmane A, Vassoille R. Colloid Polym Sci 1992;270:1182.
[18] Ivanov DA, Jonas AM. J Polym Sci: Part B: Polym Phys 1998;36:919.
[19] Ivanov DA, Legras R, Jonas AM. Macromolecules 1999;32:1582.
[20] Jonas A, Legras R. Macromolecules 1993;26:4489.
[21] Ruland W. Colloid Polym Sci 1977;255:417.
[22] Koberstein JT, Morra B, Stein RS. J Appl Cryst 1980;13:34.
[23] Glatter O. J Appl Cryst 1974;7:147.
[24] Strobl GR, Schneider M. J Polym Sci: Part B 1980;18:1343.
[25] Fougnies C, Damman P, Dosière M, Koch MH. Macromolecules 1997;30:1392.
[26] Kalika DS, Gibson DG, Quiram DJ, Register RA. J Polym Sci: Part B 1998;36:65.
[27] Jonas AM, Ivanov DA, Yoon DY. Macromolecules 1998;31:5352.
[28] Glatter O, Kratky O. Small angle X-ray scattering, London: Academic Press, 1982.
[29] Veeraraghavan VG, Rubin H, Winchell PG. J Appl Cryst 1977;10:66.
[30] Medellin-Rodriguez FJ, Phillips PJ, Lin JS. Macromolecules 1995;28:7744.
[31] Blundell DJ, Osborn BN. Polymer 1983;24:953.
[32] Day M, Deslandes Y, Roovers J, Suprunchuk T. Polymer 1991;32:1258.
[33] Nichols ME, Robertson RE. J Polym Sci: Part B: Polym Phys 1992;30:755.
[34] Hay JN, Langford JI, Lloyd JR. Polymer 1989;30:489.
[35] Wakelyn NT. J Polym Sci: Polym Lett 1987;25:25.
[36] Deslandes Y, Alva Rosa E. Polym Commun 1990;31:269.
[37] Ivanov DA, Jonas AM. Macromolecules 1998;31:4546.
[38] Balta-Calleja FJ, Vonk CG. X-ray scattering of synthetic polymers, Amsterdam: Elsevier, 1989.
[39] Lee Y, Porter RS, Lin JS. Macromolecules 1989;22:1756.
[40] Lee Y, Porter RS. Macromolecules 1987;20:1336.
[41] Dupont O, Jonas AM, Legras R. J Appl Cryst 1997;30:921.